Electronic Supplementary Material (ESI) for Chemical Science

Supporting Information

Selective CO_2 Uptake and Inverse CO_2/C_2H_2 selectivity in a Dynamic Bi-Functional Metal-Organic Framework

Wenbin Yang[a] Andrew J. Davies,[a] Xiang Lin,[a] Mikhail Suyetin, [a] Ryotaro Matsuda,[b] Alexander J. Blake,[a] Claire Wilson,[a] William Lewis,[a] Julia E. Parker,[c] Chiu C. Tang,[c] Michael W. George,[a] Peter Hubberstey,[a] Susumu Kitagawa,[b] Hirotoshi Sakamoto,[b] Elena Bichoutskaia, [a] Neil R. Champness,[a] Sihai Yang[a]* and Martin Schröder[a]*

[a] School of Chemistry, University of Nottingham, University Park, Nottingham NG7 2RD, United Kingdom. Corresponding authors: Sihai.Yang@nottingham,ac.uk, +44 (0)115 9513452; m.schroder@nottingham.ac.uk, +44 (0)115 9513512

[b] ERATO Kitagawa Integrated Pores Project, Science and Technology Agency (JST), Kyoto Research Park Bldg#3, Shimogyo-ku, Kyoto, 600-8815, Japan, and Institute for Integrated Cell-Material Science (iCeMS), Kyoto University, Yoshida, Sakyo-ku, Kyoto 606-8501, Japan.

[c] Diamond Light Source, Harwell Science and Innovation Campus, Didcot, Oxfordshire, OX11 0DE, UK.

1. Additional experiment details

All reagents were used as received from commercial suppliers without further purification. Elemental analyses of C, H and N were performed by the Elemental Analysis Service of the School of Chemistry, University of Nottingham. Infrared spectra were measured as KBr disks on a Nicolet Avatar 360 FT-IR system over the 400-4000 cm^{-1} range. Thermogravimetric analysis (TGA) was performed on a Rheometric Scientific STA 1500H thermal analyzer at a heating rate of 1ºC/min^{-1} under N_2 flow. In-house X-ray powder diffraction data were collected on a Philips X'pert powder diffractometer with Cu-K_α radiation using a plate sample holder at room temperature.

2. Measurements of gas isotherms

The N_2, CO_2, CH_4 and H_2 isotherms were determined using an IGA gravimetric adsorption apparatus at the University of Nottingham, in a clean ultrahigh vacuum system with a diaphragm and turbo pumping system. Ultrapure plus grade (99.9995%) H_2 was purified further using calcium aluminosilicate and activated carbon adsorbents to remove trace amounts of water and other impurities before introduction into the IGA system. For measurements at liquid nitrogen temperature, a standard low-temperature liquid Dewar vessel was used. Before gas absorption measurements, the sample was thermally activated at 125 ^{o}C under ultrahigh vacuum (10^{-8} mbar) for at least 12h. About 50 mg of sample was loaded for gas adsorption and the weight of each sample was recorded before and after outgassing to confirm full removal of guest molecules. A typical weight loss of ~16-20wt% was observed during the outgassing porcess, consistent with the TGA results. The volatility of crystallization solvents in the samples contributes to the discrepancies between TGA and IGA results. This is attributable to small losses of volatile solvent during procedures of loading and weighing of samples. All isotherm data points were fitted by the IGASwin system software v.1.03.143 (Hiden Isochema, 2004) using a linear driving force model when > 98% equilibration had been reached. A maximum equilibration time of 4 hours for each pressure step was set. The typical equilibration time for H_2 or CH_4 uptake is less than 10 minutes. The equilibration time for other gas uptakes are ~30-60 minutes for each step. All the isotherm points were checked to ensure that they reached equilibrium. All changes in sample weight were corrected for buoyancy effects. Acetylene adsorption isotherms at 195 K were recorded on BELSORP-max volumetric adsorption equipment from Bel Japan, Inc. Acetylene gas of high purity (> 99.9999%) was used. Each point in the adsorption isotherm has an error of ± 0.25 %, which is caused by the resolution of the pressure gauge.

3. Structure description of [Co(HL^{dc})]·2DMF·H$_2$O (2)

The solvothermal reaction of H$_4$L with Co(NO$_3$)$_2$·6H$_2$O in DMF at 90°C afforded [Co(HL^{dc})]·2DMF·H$_2$O (**2**), as purple tablet crystals. Compound **2** crystallizes in the triclinic space group *P*-1, and its asymmetric unit contains two crystallographically-independent Co(II) ions each exhibiting tetrahedral coordination by two monodentate carboxylate units and two pyridyl N-donors from four different [HL^{dc}]$^{2-}$ ligands (Fig. S3). It should be pointed out that rotational disorder occurs on some functional moieties in each [HL^{dc}]$^{2-}$ ligand. Although the asymmetric unit of **2** and the co-ordination spheres of Co(II) are different from those observed for **2**, both complexes exhibit the same connectivity between Co(II) centres and [HL^{dc}]$^{2-}$ ligands. Consequently, (HL^{d})$^{2-}$ ligands in **2** bridge metal centers to form a 3D (3,4)-connected (8^3)$_2$(8^6)-**tfa** network, as observed for **1**. However, the positional disorder of free uncoordinated carboxyl group leads to a subtle change of the shapes of carboxyl-functionalized channels (Fig. S3).

4. Bond valence sum (BVS) calculations for 1 and assignments of the protonated state of (HL^{dc})$^{2-}$

A bond-valence model based on the Brown equation (1)[1] was applied to assess the oxidation state of the cobalt ions in **1**, and the results of the calculations are shown in Table S3.

$$V_i = \sum_j V_{ij} = \sum_j \exp\left(\frac{r_o^{'} - r_{ij}}{B}\right) \qquad (1)$$

where V_{ij} is the valence of a bond between two atoms, *i* and *j*; V_i is the atom valence of a given atom, *i*, which is equal to the sum of all bond valences of the bonds formed by the given atom, *i*. r_0 is an empirical parameter determined for pairs of atoms. r_{ij} is the bond length between atoms *i* and *j*. In this work, *i* and *j* are Co and O or Co and N (for Co-O, r_0 = 1.70 Å; for Co-N, r_0 = 1.84 Å). B is a constant, the "universal parameter" ~0.37 Å.

Bond valence sum (BVS) calculations allows assignment of the metal center oxidation state in **1** as Co(II) ($\sum$s values, 2.111). Therefore, either the unco-ordinated carboxylate group or the unco-ordinated pyridyl nitrogen centre is in a protonated form. We assign the unco-ordinated carboxylate group as being in its protonated form, i.e. as a carboxylic acid, based upon the significant difference in two C-O distances [1.343(8) Å *vs.* 1.221(7) Å] of the unbound carboxyl group and the successful location of the H atom on this group from Fourier synthesis.

5. Analysis of gas adsorption isotherms

A Langmuir plot was used to estimate the maximum uptake of various gases under their isothermal conditions.

$$\frac{P}{W} = \left(\frac{1}{W_0}\right)P + \frac{1}{W_0 K} \qquad (2)$$

$$\text{Converted into Y = A + B*X, } W_0 = 1/\text{B} \qquad (3)$$

where W is the amount adsorbed at the pressure of P, W_0 is the amount adsorbed at saturation, and K is a coefficient. Based on the Langmuir plot to the sorption data, we can obtain the saturation amount, W_0 = 1/B. Once W_0 is obtained, the pore volume and Langmuir surface area of porous materials can be calculated using the expressions:

$$V_P = \frac{W_0}{\rho_{\text{liqud}}} \qquad (4)$$

$$S\,(\text{m}^2/\text{g}) = \frac{6.023 \text{ x } 10^{23}\,\sigma\; V_0}{22414 \text{ cm}^3 \text{ x } (10^{18} \text{ nm}^2 / \text{m}^2)} \qquad (5)$$

where W_0 (g/g) is the saturated adsorption amount obtained from Langmuir plots, ρ_{liquid} is the density of pure liquid absorbates [$\rho(N_2$, 77K) = 0.808 g cm^{-3}; $\rho(CO_2$, 253 K) = 1.032 g cm^{-3}];[2] σ is the molecular cross-sectional area of the gas (*i. e.* 0.170, 0.187 and 0.195 nm^2 for CO_2 at 196 K, 273K and 298 K, respectively);[3] V_0 is the monolayer capacity (cm^3 g^{-1}) that corresponds to W_0 (g/g or wt%).

The isotherms were analysed using the Dubinin-Radushkelvich (DR) equation[4] [*eq.* (6)] to define the porosity of the material. In the high relative pressure (P/P_0) region, the DR plot has a linear relationship which was used to deduce the adsorption energy βE_0 and the isosteric heat of gas adsorption.

$$\ln W = \ln W_0 - \left(\frac{RT}{\beta E_0}\right)^2 \left(\ln\left(\frac{P_0}{P}\right)\right)^2 \qquad (6)$$

Converted into Y = A + B*X

$$\beta E_0 = (RT)/(-B)^{1/2} \qquad (7)$$

$$q_{st,\ \Phi = 1/e} = \Delta H_v + \beta E_0 \qquad (8)$$

where the ΔH_V of the gas at its boiling point was used (N_2 = 5.55 kJ mol^{-1} at 77.36 K; H_2 = 0.91 kJ mol^{-1} at 20.39 K; C_2H_2 = 20.87 kJ mol^{-1} at 189.3 K; CO_2 = 25.13 kJ mol^{-1} at 194.6 K).[2]

6. Estimation of H_2 adsorption enthalpies

In Virial Method,[5,6]

$$\ln(n/p) = A_0 + A_1 n + A_2 n^2 ..... \qquad (9)$$

where p is pressure (Pa), n is amount (mol g^{-1}) adsorbed, and A_0, A_1, A_2 etc. are virial coefficients. At low surface coverage A_2 and higher terms can be neglected. The van't Hoff isochore was used to determine the isosteric enthalpy of adsorption at specific surface coverages. The isosteric enthalpies of adsorption at zero surface coverage were obtained from the A_0 values.

7. Estimation of free-energy difference (ΔF_{host}) between *np* and *lp* forms for CO_2 adsorption

To calculate the free-energy difference (ΔF_{host}) between the two guest-free forms, we applied the modified equation (12), which can be derived from the thermodynamic model recently developed to model the CO_2 isotherms for MIL-53[7,8] and DMOF-1-AM[9] materials. The thermodynamic potential Ω_{os} can be expressed by equation (12).

$$\Omega_{os}(T,P) = F_{host}(T) + PV - \int_0^p N_{ads}(T,P)V_m(T,P)dP \qquad (10)$$

Because during the phase transition process:

$$\Delta\Omega_{os}(P_{trans}) = 0 \quad \text{and} \quad P_{trans}\Delta V \approx 0$$

The equation (10) can be re-arranged to give (11)

$$\Delta F_{host}(T) = \int_0^{p_{trans}} {}^2N_{ads}(P)V_m(P)dP - \int_0^{p_{trans}} {}^1N_{ads}(P)V_m(P)dP \qquad (11)$$

Using the LF equation and universal gas equations:

$$ {}^{i}N_{ads} = \frac{{}^{i}N_{\max} K_i P^{1/n_i}}{1 + K_i P^{1/n_i}} \quad \text{and} \quad V_m(P) = RT/P $$

equation (11) can be re-arranged to give (12)

$$ \Delta F_{host} = RT\left[n_2\, {}^{2}N_{\max} \ln(1 + K_2 P_{trans}^{1/n_2}) - n_1\, {}^{1}N_{\max} \ln(1 + K_1 P_{trans}^{1/n_1}) \right] \qquad (12) $$

8. Additional Tables

Table S1. Summary of crystal data and structure refinement for {[Co(HL^{dc})]·1.5MeOH·dioxane}$_n$ (**1**) and {[Co(HL^{dc})]·2DMF·H_2O}$_n$ (**2**).

Complexes	**1**	**2**
Chemical Formula	$C_{35.50}H_{31}Co\ N_3O_{9.50}$	$C_{72}H_{66}Co_2N_{10}O_{18}$
FW	710.56	1477.21
Crystal size (mm^3)	0.34 x 0.15 x 0.14	0.23 x 0.18 x 0.10
Space group	$P2_1/c$	P-1
a (Å)	12.565(2)	10.090(2)
b (Å)	29.618(5)	16.362(3)
c (Å)	9.858(2)	24.453(5)
α (^{o})	90	106.75(3)
β (^{o})	105.695(3)	92.97(3)
γ (^{o})	90	103.16(3)
V (Å^3)	3531.9(11)	3734(2)
ρ_{calcd} (g/cm^3)	1.336	1.314
θ_{min}, θ_{max} (^{o})	2.25, 26.37	2.3, 27.35
μ (mm^{-1})	0.534	0.518
F(000)	1472	1532
no. of reflns	20276	33315
no. of unique reflns	7379	16720
no. of obsd reflns [$I>2\sigma(I)$]	4137	8858
no. of paras	405	720
R_{int}	0.064	0.044
R_1, wR_2	0.114, 0.298	0.0752, 0.118
GOF	1.046	0.95
Max./ Min. residuals (eÅ^{-3})	2.00 / -0.63	1.60 / -0.73

Table S2. Selected inter-atomic distances and angles for **1** and **2**.

	1[a]		
Co(1)-O(1)	1.956(5)	O(1)-Co(1)-O(3)#1	92.2(2)
Co(1)-O(3)#1	1.999(5)	O(1)-Co(1)-N(3)#2	107.0(2)
Co(1)-N(3)#2	2.037(6)	O(3)#1-Co(1)-N(3)#2	121.9(3)
Co(1)-N(2)#3	2.073(5)	O(1)-Co(1)-N(2)#3	112.9(3)
Co(1)-O(4)#1	2.385(6)	O(3)#1-Co(1)-N(2)#3	112.2(2)
O(1)-C(1)	1.235(10)	N(3)#2-Co(1)-N(2)#3	109.4(2)
O(2)-C(1)	1.252(9)	O(1)-Co(1)-O(4)#1	149.7(2)
O(4)-C(8)	1.246(9)	O(3)#1-Co(1)-O(4)#1	58.2(2)
O(5)-C(20)	1.220(8)	N(3)#2-Co(1)-O(4)#1	86.3(2)
O(6)-C(20)	1.337(9)	N(2)#3-Co(1)-O(4)#1	86.6(2)
	2[b]		
Co(1)-O(1)	1.979(3)	O(3)#1-Co(1)-O(1)	96.24(10)
Co(1)-O(3)#1	1.972(2)	O(3)#1-Co(1)-N(6)	119.08(12)
Co(1)-N(6)	2.028(5)	O(1)-Co(1)-N(6)	109.64(12)
Co(1)-N(2)#2	2.047(5)	O(3)#1-Co(1)-N(2)#2	105.99(12)
Co(2)-O(9)	1.968(3)	O(1)-Co(1)-N(2)#2	113.75(13)
Co(2)-O(12)#3	1.971(3)	N(6)-Co(1)-N(2)#2	111.45(12)
Co(2)-N(3)#5	2.042(3)	O(9)-Co(2)-O(12)#3	97.04(12)
Co(1)-N(5)#4	2.057(3)	O(9)-Co(2)-N(3)#5	117.49(13)
C(30)-O(5)	1.275(15)	O(12)#3-Co(2)-N(3)#4	112.79(13)
C(30)-O(6)	1.366(14)	O(9)-Co(2)-N(5)#4	105.97(13)
C(31)-O(8)	1.268(9)	O(12)#3-Co(2)-N(5)#4	112.92(13)
C(31)-O(7)	1.357(10)	N(3)#5-Co(2)-N(5)#4	110.02(13)
O(14)-C(61)	1.305(11)		
O(15)-C(62)	1.247(11)		
O(16)-C(62)	1.287(11)		

[a] Symmetry transformations used to generate equivalent atoms: #1 x,y,z+1; #2 -x+3,y+1/2,-z+3/2; #3 -x+2,y+1/2,-z+3/2.

[b] Symmetry transformations used to generate equivalent atoms: #1 x-1,y,z; #2 x-1,y-1,z; #3 x+1,y,z; #4 x,y-1,z+1; #5 x,y-1,z.

Table S3. BVS calculation for **1** and **2**.

compounds	Atom-atom	length (Å)	V_{ij}	$V_i = \sum V_{ij}$
1[a]	Co(1)-O(1)	1.956(5)	0.501	2.111
	Co(1)-O(3)#1	1.999(5)	0.446	
	Co(1)-N(3)#2	2.037(6)	0.402	
	Co(1)-N(2)#3	2.073(5)	0.533	
	Co(1)-O(4)#1	2.385(6)	0.229	
2[b]	Co(1)-O(1)	1.979(3)	0.470	2.123
	Co(1)-O(3)#1	1.972(2)	0.479	
	Co(1)-N(6)	2.028(5)	0.602	
	Co(1)-N(2)#2	2.047(5)	0.572	
	Co(2)-O(9)	1.968(3)	0.485	2.101
	Co(2)-O(12)#3	1.971(3)	0.481	
	Co(2)-N(3)#5	2.042(3)	0.579	
	Co(2)-N(5)#4	2.057(3)	0.556	

[a] Symmetry transformations used to generate equivalent atoms: #1 x,y,z+1; #2 -x+3,y+1/2,-z+3/2; #3 -x+2,y+1/2,-z+3/2.

[b] Symmetry transformations used to generate equivalent atoms: #1 x-1,y,z; #2 x-1,y-1,z; #3 x+1,y,z; #4 x,y-1,z+1; #5 x,y-1,z.

Table S4. Porosity parameters for **1a**, with calcd. density: 1.08 g cm^{-3}, accessible voids: 38.0 %, and calcd. pore volume: 0.352 ml g^{-1} by *PLATON*.

Adsorbates	Uptake [wt%] ([mmol/g])	P_e[a] [bar]	Analytical Method	W_0[b] [wt%]	V_P[c] [cm^3 g^{-1}]	S_A[d] [m^2 g^{-1}]	βE_0[e] [kJ/mol]	$Q_{st,\Phi=1/e}$[f] [kJ/mol]
N_2 at 77 K	22.42 (8.00) 23.64 (8.44) 26.45 (9.44)	0.01 0.10 0.95	Langmuir	26.86	0.332	936	-	-
			DR	$W_{0,e}$ = 23.71 $W_{0,t}$ = 26.51	0.328	-	14.22 5.04	19.77 10.59
			BET	22.19		773	-	-
CO_2 at 195 K	25.69 (5.84) 30.45 (6.92) 47.02 (10.68)	0.01 0.10 1.00	Langmuir	49.14	0.476	1143	-	-
			DR	$W_{0,e}$ = 34.06 $W_{0,t}$ = 46.95	0.294 0.455	-	15.32 8.28	40.45 33.41
			BET	34.78	-	809	-	-

[a] P_e-adsorption equilibrium pressures corresponding to the gas uptakes; [b] W_0 – the uptake estimated from Langmuir, BET or DR plots; [c] V_P – Pore volume, $V_P = W_0/\rho_{liquid}$ where W_0 and ρ_{liquid} are the saturation uptake and density of pure liquid absorbates ($\rho(N_2, 77K) = 0.808$ g cm^{-3}; $\rho(CO_2, 253\ K) = 1.032$ g cm^{-3}). [d] $\boldsymbol{S}_A$ – Surface area, calculated with formula: $\boldsymbol{S}_A$ (m^2 g^{-1}) = $[6.023 \times 10^{23}\sigma \boldsymbol{V}_0]/[22414\ \text{cm}^3 \times (10^{18}\ \text{nm}^2\ \text{m}^{-2})$, where σ is the molecular cross-section area of gases used [$\sigma(N_2, 77\ K) = 0.162$ nm^2, $\sigma(CO_2, 196\ K) = 0.170$ nm^2], and V_0 is the monolayer capacity (cm^3/g) corresponding to W_0. [e] βE_0 –the adsorption energy, obtained from Dubinin-Radushkevich (DR) analysis. [f] $Q_{st,\Phi=1/e} = \beta E_0 + \Delta H_V$, where the ΔH_V of gases at their boiling point was used (N_2 = 5.55 kJ mol^{-1} at 77.36 K; CO_2 = 25.13 kJ mol^{-1} at 194.6 K).

Table S5. Summary of H_2, CH_4 and C_2H_2 storage data for **1a**.

Absorbates (measured temperature)	$\boldsymbol{W}_A$ [a] [wt%] (mmol/g)	$\boldsymbol{D}_A$ [b] [$\times 10^{-2}$ g/cm^3]	$\boldsymbol{P}c$ [c] [bar]	$\boldsymbol{W}_0$[d] [wt%] (cm^3 g^{-1})	$\boldsymbol{D}_V$ [e] [g L^{-1}]
C_2H_2 (195 K)	10.85 /13.39 / 16.16 (4.17 / 5.14 / 6.21)	30.82 / 38.04 / 45.91	0.01/ 0.10/ 1.0	16.62 (143.68)	179.51
CH_4 (195 K)	5.58 / 8.22 / 9.92 (3.48 / 5.13 / 6.18)	15.85 / 23.35 / 28.18	0.2 / 1.0 / 10.0	10.17 (142.05)	109.84
H_2 (77 K)	1.18 / 1.62 / 2.28 (5.85 / 8.02 / 11.29)	3.35 / 4.60 / 6.48	0.2 / 1.0 / 20.0	2.36 (261.93)	25.48
H_2 (88 K)	0.81 / 1.30 / 2.02 (4.01 / 6.45 /10.03)	2.30 / 3.69 / 5.74	0.2 / 1.0 / 20.0	2.11 (234.83)	22.78

[a] $\boldsymbol{W}_A$ – the adsorbed amount; [b] $\boldsymbol{D}_A$ – the absorbed density, Calculated with the absorbed values ($\boldsymbol{W}_A$) and the accessible crystal volume $\boldsymbol{V}_{PLAT}$ (0.352 cm^3/g); [c] $\boldsymbol{P}_c$ – the pressure conditions corresponding to the above adsorbed amounts; [d] $\boldsymbol{W}_0$ – the saturation adsorbed amount obtained from Langmuir plots; [e] $\boldsymbol{D}_V$ –the volumetric density of adsorbed gases, obtained by using equation of $\boldsymbol{D}_V = \boldsymbol{W_0} * \boldsymbol{D}_{calcd}$, where $\boldsymbol{D}_{calcd}$ is the calculated density (1.08 g/cm^3) of desolvated solid of **1**, and $\boldsymbol{W}_0$ has the same definition as above.

Table S6. Summary of the Langmuir-Freundlich fit to the CO_2 sorption isotherm at 195 K for **1a**.

Langmuir-Freundlich Fit Parameters						P_{trans}(Pa)		ΔF_{host}(kJ/mol)
lp phase			***np*** phase					
$^2N_{max}$ (mol/mol)	K_2(Pa^{-1})	n_2	$^1N_{max}$ (mol/mol)	K_1(Pa^{-1})	n_1			
R^2=0.98			R^2=0.99					
6.228	7.57e^{-5}	0.858	4.122	0.0556	1.590	Adsorption	12500	16.6
						Desorption	8300	8.3

9. Additional Figures

By depicting the metal center as well as the ligand $(HL^{dc})^{2-}$ as 4-connecting polyhedra, the structure of the MOF **1a** is reduced to a modified diamond net with Schlafli notation of $(6^6)_{ligand}(6^6)_{metal}$ as shown in Fig. S1.

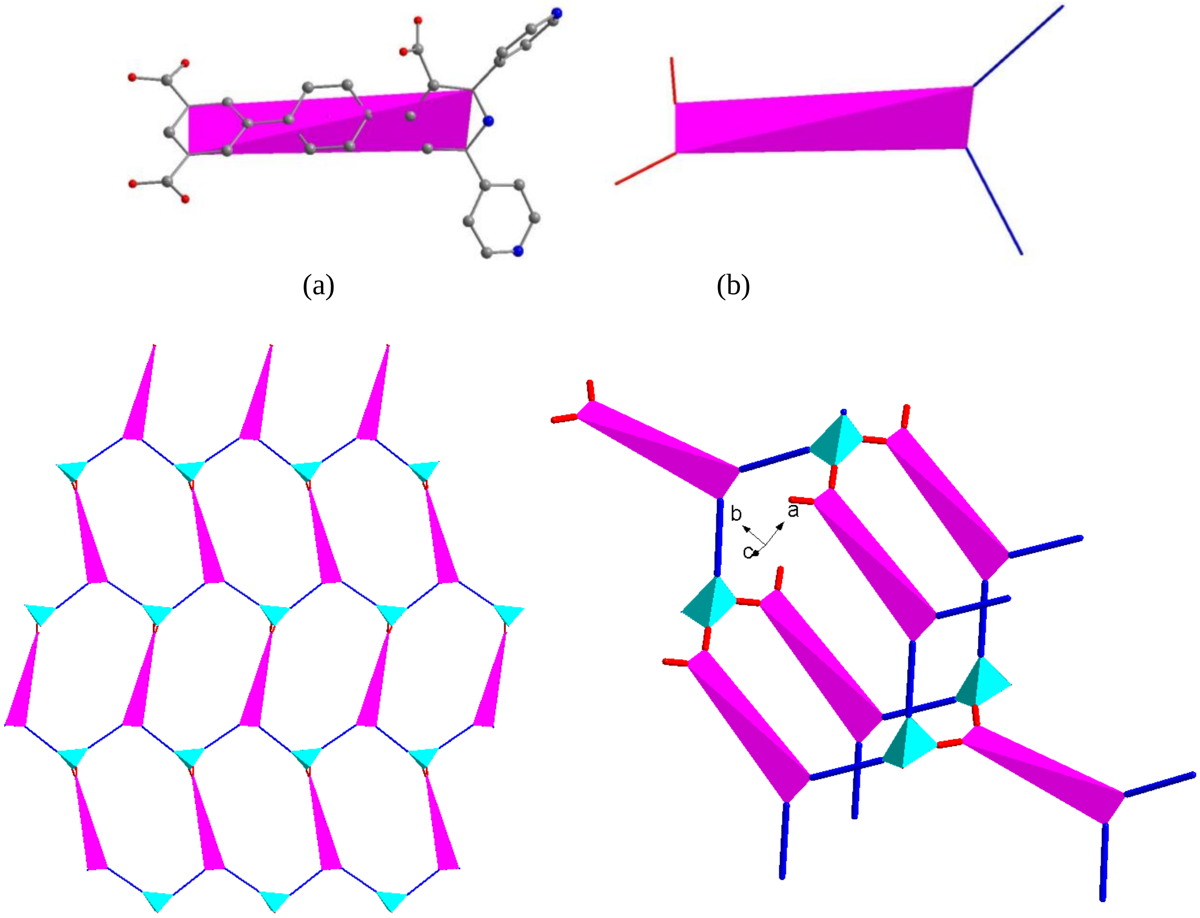

(a) (b)

(c) (d)

Figure S1. Views of topological nets in **1**. (a) and (b) Views of the topology of $[HL^{dc}]^{2-}$ in **1**; (c) view of modified diamond net in **1** depicting the $[HL^{dc}]^{2-}$ ligand as a distorted 4-connecting tetrahedron (purple) and the metal as a 4-connecting tetrahedral node (green); (d) a representative adamantoid unit in the modified diamond net of **1**. The red lines represent the linkage between ligand and metal nodes via carboxylate groups, while blue lines are the linkages between ligand and metal node *via* pyridyl groups.

Alternatively, $(HL^{dc})^{2-}$ can be described as a pair of 3-connecting nodes; one node one is the phenyl ring of isophthalate moiety and the other is the internal pyridyl ring of the terpy unit and these are linked together *via* the phenyl spacer. Thus the overall network of **1** is topologically equivalent to a 3D (3,4)-connected $(8^3)_2(8^6)$ **tfa** net (Fig. S2), with the full vertex symbol of $(8^4{\cdot}8^4{\cdot}8^4)_2(8^2{\cdot}8^2{\cdot}8^3{\cdot}8^3{\cdot}8^3{\cdot}8^3)$.

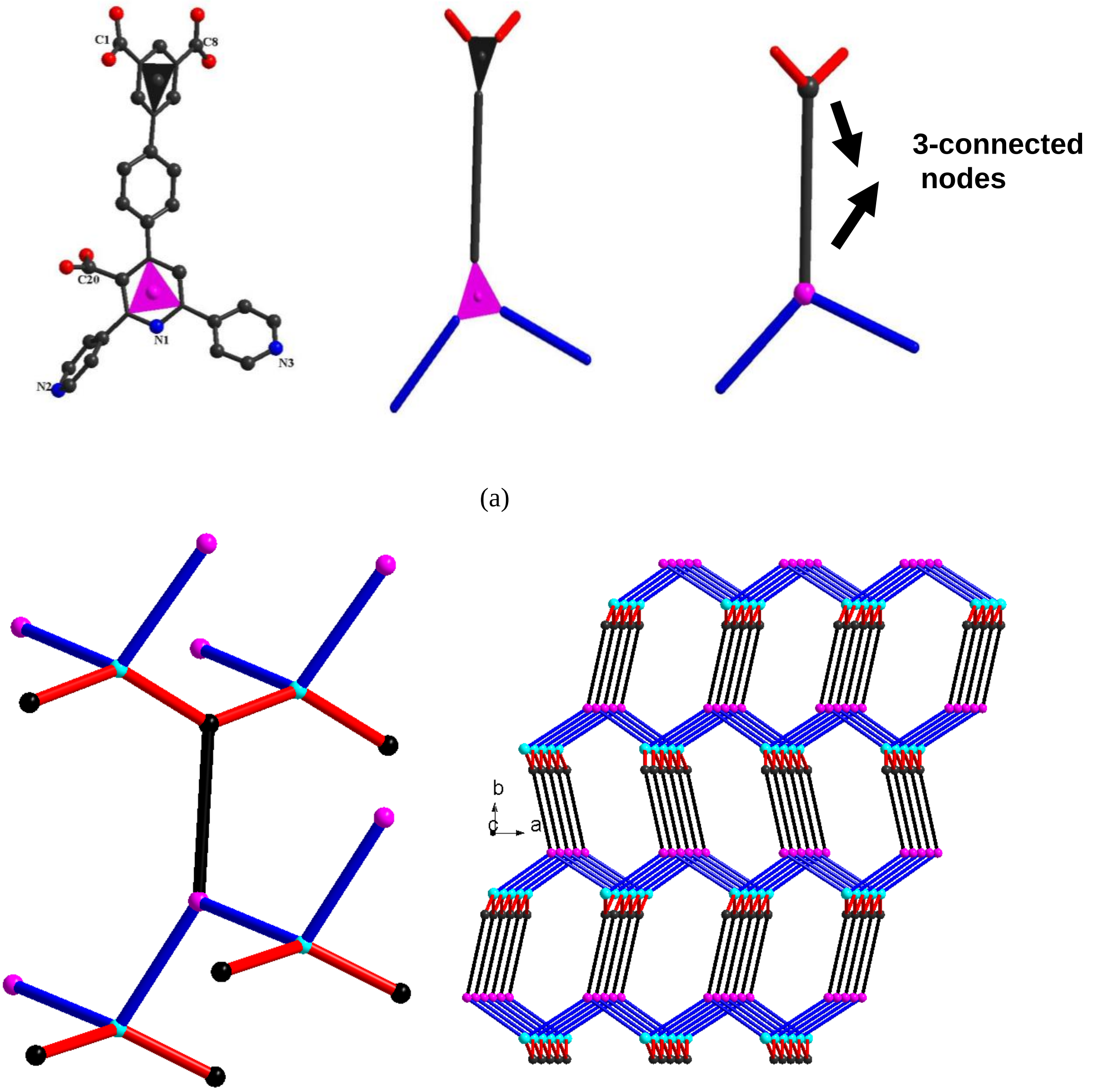

(a)

(b)

(c)

Figure S2. Topological network of **1**. (a) Each $(HL^{dc})^{2-}$ ligand can be described as a pair of 3-connecting nodes: one is on the phenyl ring (shown as a black ball) of the isophthalate moiety, the other (shown as a purple ball) is on the internal pyridyl ring of the terpy unit; (b) 3,4-connectivity in the network of **1**. (c) (3,4)-connected $(8^3)_2(8^6)$ **tfa** network of **1**. The red lines represent the linkage between ligand node and metal node via carboxylate groups, while blue lines are the linkage between ligand node and metal node *via* pyridyl groups, and the black lines are the linkage between 3-connecting nodes *via* the phenyl spacer.

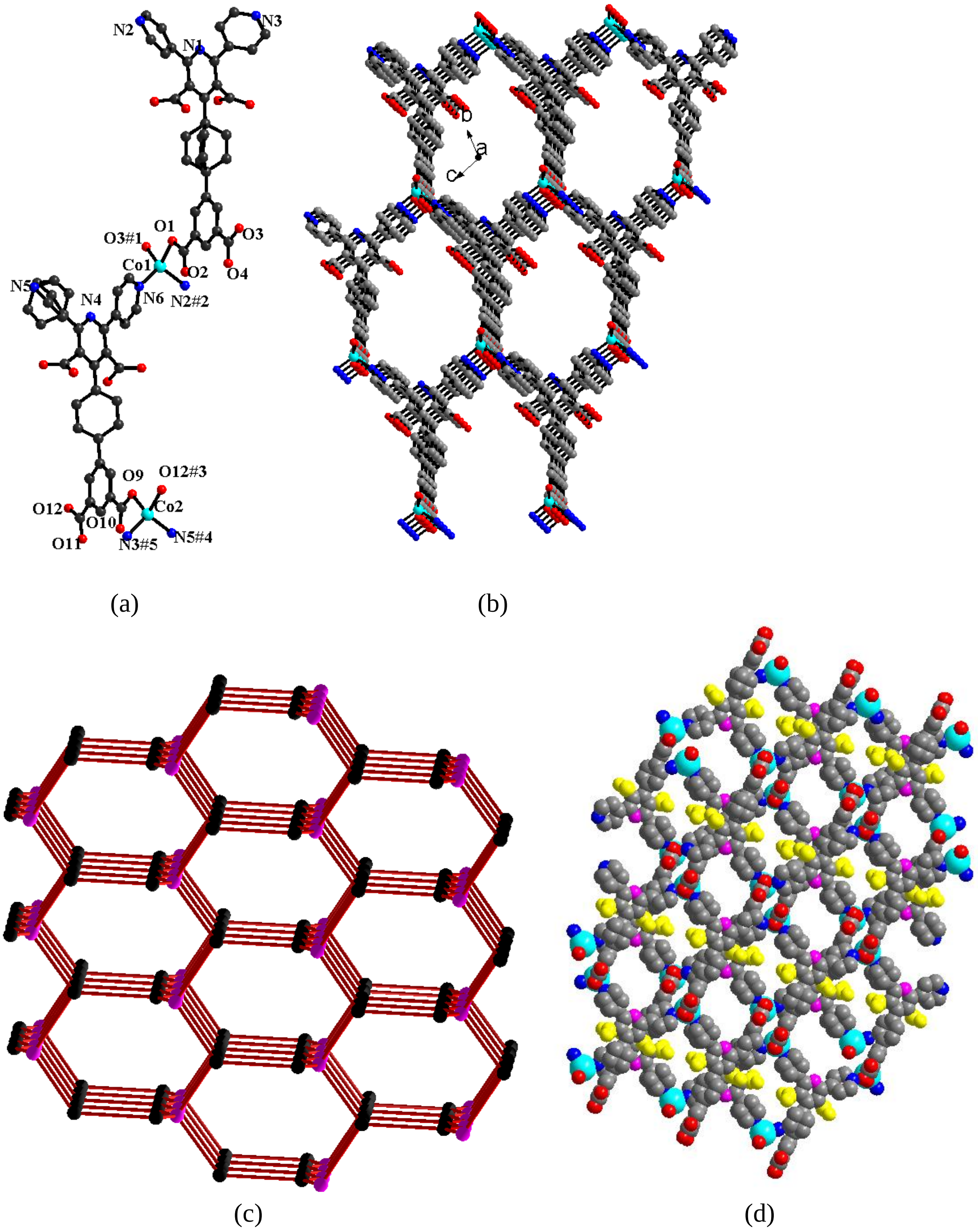

(a) (b)

(c) (d)

Figure S3. Crystal structure of **2**. (a) Coordination geometry at Co(II) in **2** (the occupancy ratio of free carboxylic groups at 3'- and 5'-positions of the 4,2':6',4"-terpyridine moiety is 0.5); (b) Perspective view of the 3D (3,4)-connected nanoporous framework of **2**; (c) a (3,4)-connected $(8^3)_2(8^6)$-**tfa** net for **2**; (d) space-filling views showing functional channels in **2**. Highlighted colour modes: free uncoordinated carboxyl groups, green; uncoordinated internal pyridyl N, purple; normal colour modes: C, dark grey; N, blue; O, red; Co, cyan).

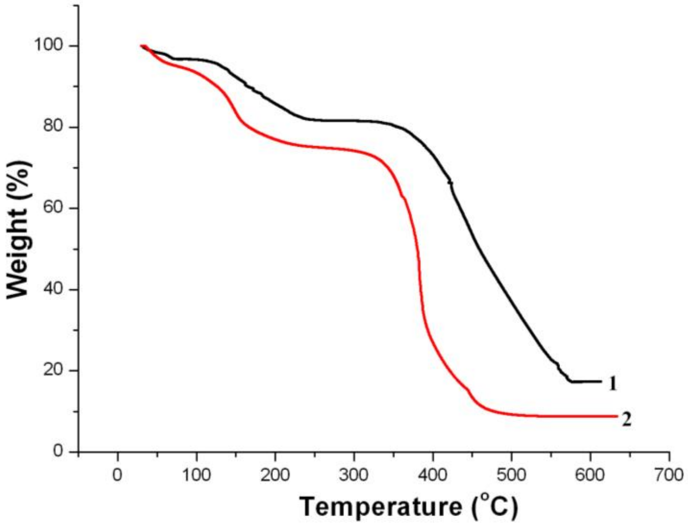

Figure S4. TGA profiles of (**1**) and (**2**).

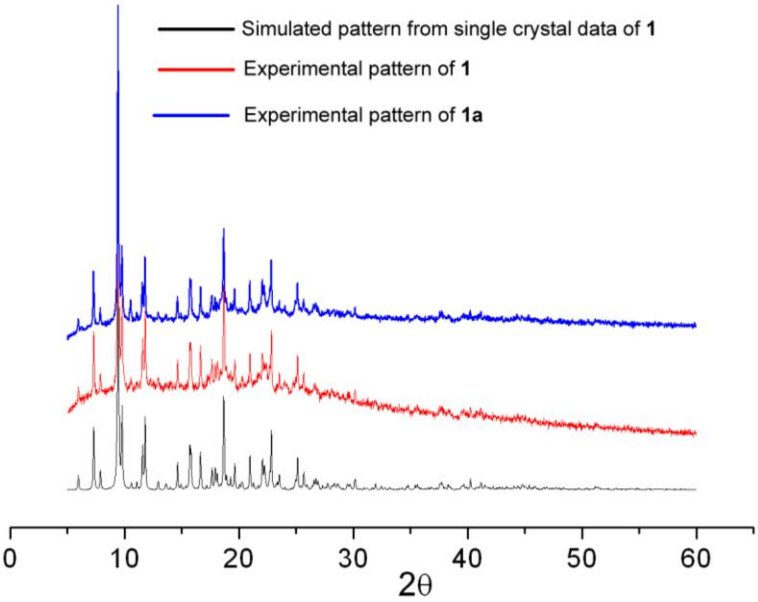

Figure S5. Comparison of PXRD patterns of **1** following thermal treatment.

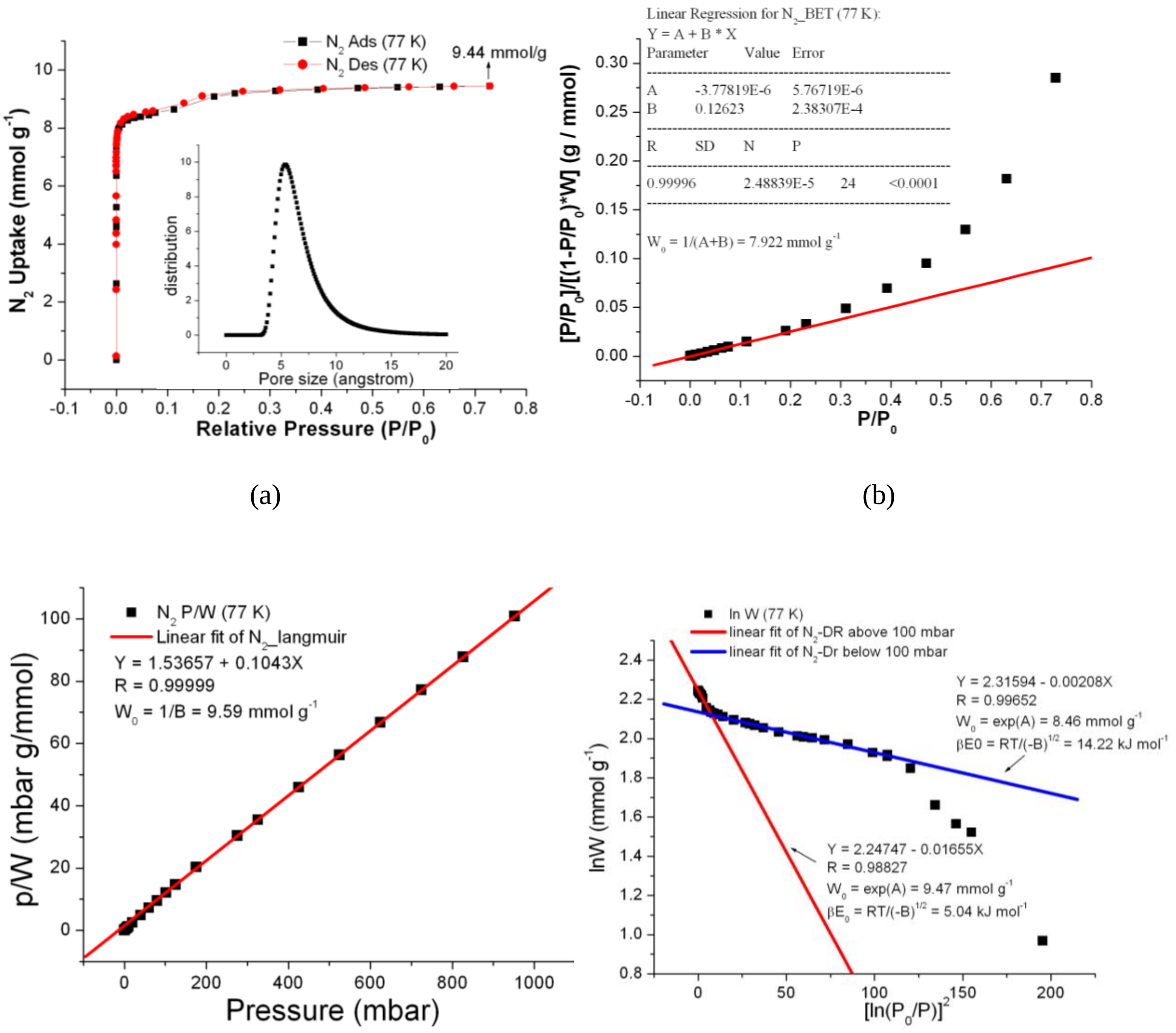

(a) (b)

(c) (d)

Figure S6. (a) N_2 isotherm of **1a** at 77 K. The inset shows the pore size distribution plot. (b) BET plots of N_2 adsorption giving $\boldsymbol{S}_{\mathrm{BET}}$ = 773 m^2/g; (c) Langmuir plot of N_2 adsorption giving $\boldsymbol{S}_{\mathrm{Lang}}$ = 936 m^2/g; (d) DR plots of N_2 adsorption giving $\boldsymbol{W}_{0,t}$ = 9.49 mmol/g (26.51 wt%) and therefore $\boldsymbol{V}$p = 0.328 cm^3/g.

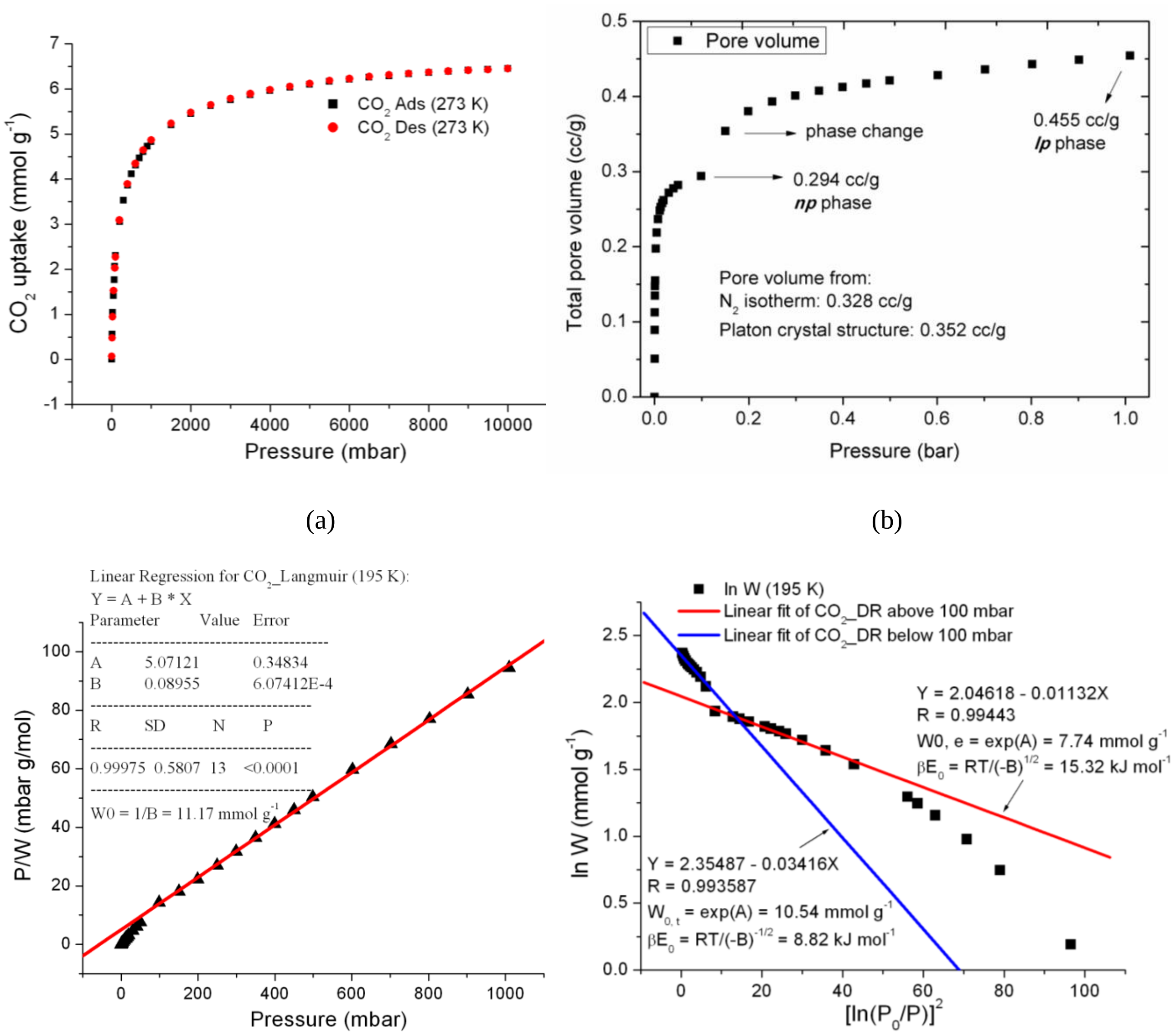

(a) (b)

(c) (d)

Figure S7. (a) CO_2 isotherm of **1a** at 273K. (b) analysis of pore volume changes on CO_2 sorption at 195 K for **1a**. (c) Langmuir plots applied to the CO_2 adsorption at 195 K, giving S_{Lang} = 1143 m^2 g^{-1}. (d) DR plots applied to the CO_2 adsorption at 195 K, $\boldsymbol{W}_{0,t}$ = 10.54 mmol/g (or 46.95 wt%) and therefore $\boldsymbol{V}$p = 0.455 cm^3/g.

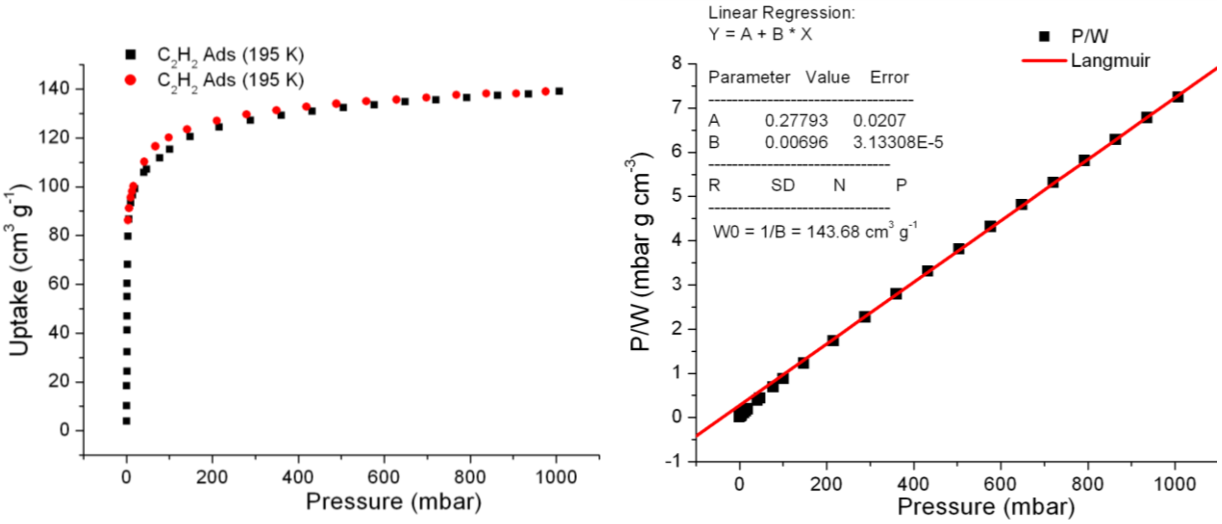

(a) (b)

Figure S8. (a) Acetylene sorption isotherm of **1a** at 195 K; (b) Langmuir plots applied to the adsorption data giving the saturation absorbed amount of 144 cm^{3}g^{-1}.

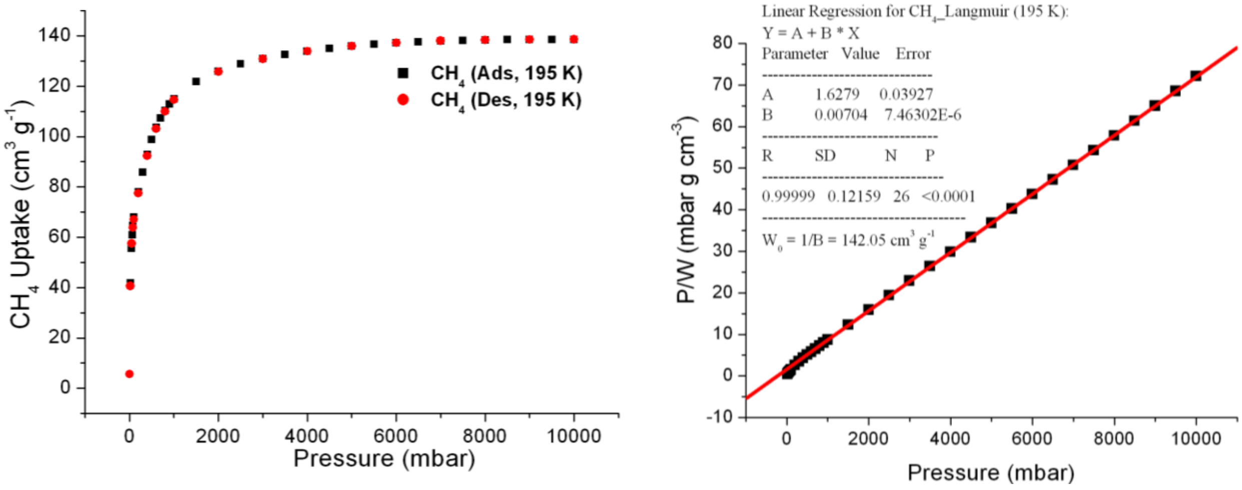

(a) (b)

Figure S9. (a) Methane isotherms of **1a** at 195 K; (b) Langmuir plots applied to the adsorption data giving the saturation absorbed amount of 142.05 cm^{3}g^{-1}.

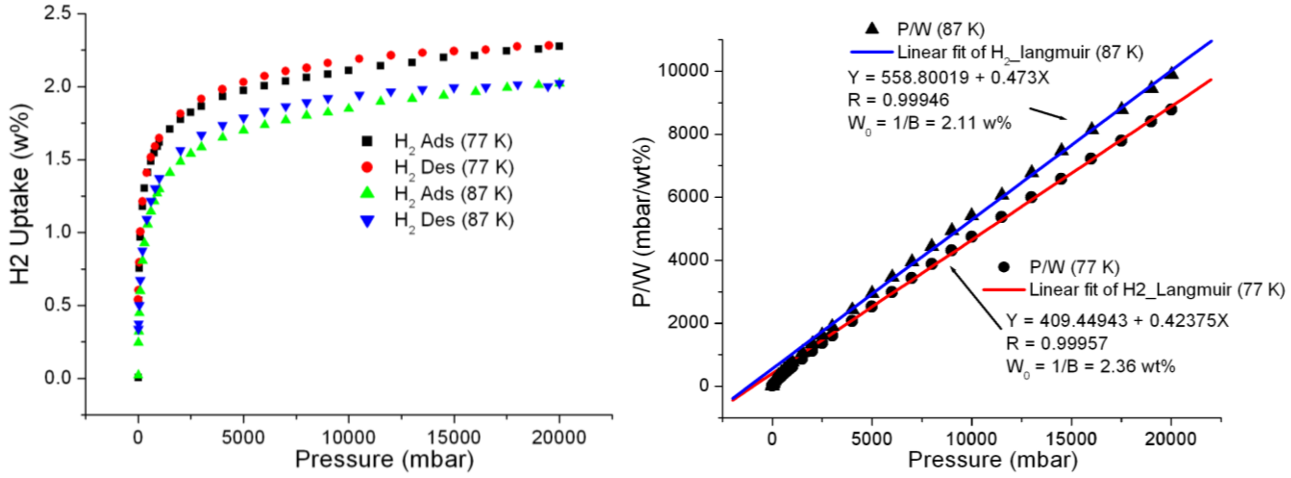

(a) (b)

Figure S10. (a) H_2 isotherms of **1a** at 77 and 87 K; (b) Langmuir plots applied to the adsorption data.

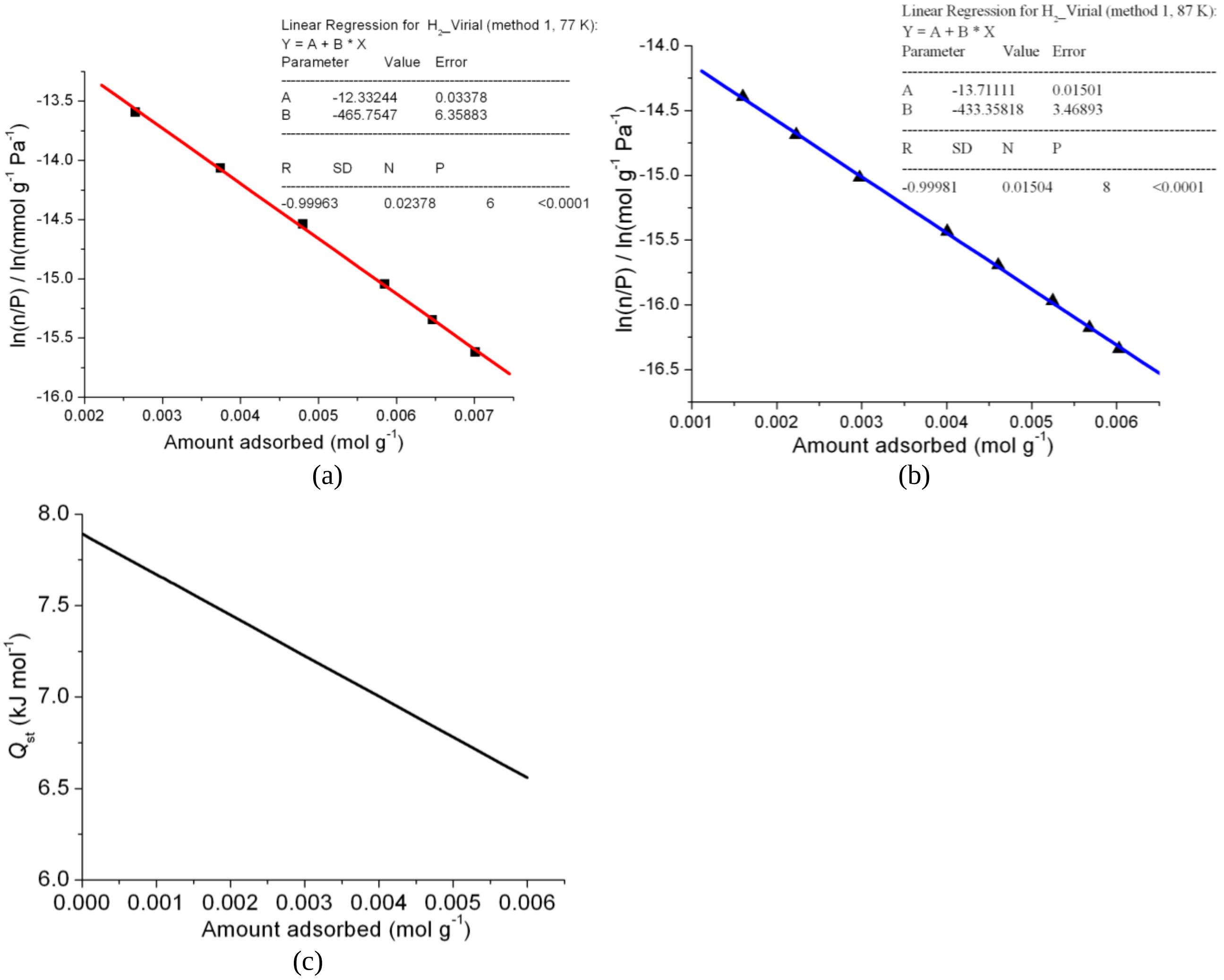

```
Linear Regression for  H2_Virial (method 1, 77 K):
Y = A + B * X
Parameter         Value    Error
------------------------------------------------------------
A         -12.33244        0.03378
B         -465.7547        6.35883
------------------------------------------------------------

R         SD        N        P
------------------------------------------------------------
-0.99963          0.02378            6          <0.0001
```

```
Linear Regression for H2_Virial (method 1, 87 K):
Y = A + B * X
Parameter         Value    Error
------------------------------------------------------------
A         -13.71111        0.01501
B         -433.35818       3.46893
------------------------------------------------------------
R         SD        N        P
------------------------------------------------------------
-0.99981          0.01504            8          <0.0001
```

(a) (b)

(c)

Figure S11. Virial fittings of the lower pressure adsorption data for H_2 on **1a** at (a) 77 K and (b) 87 K. (c) Variation of isosteric heat of adsorption with amount of adsorbed H_2 on **1a**.The isosteric heat of adsorption (Q_{st}) of H_2 for **1a** was estimated to be 7.9 kJ mol^{-1} at zero coverage.

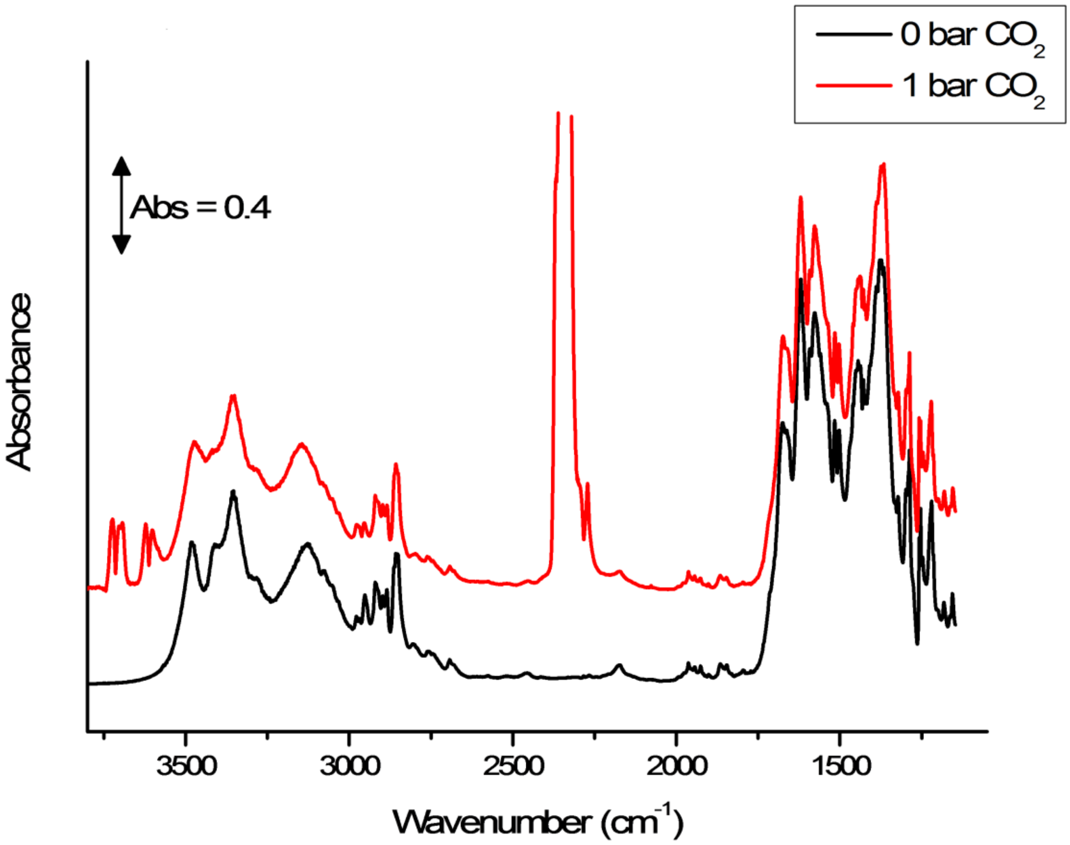

Figure S12. FTIR spectra of **1a** under vacuum (black) and in the presence of 1 bar of CO_2 (red). The spectra were recorded at 2 cm^{-1} resolution.

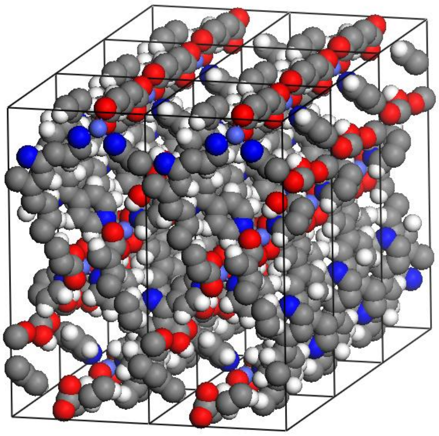

Figure S13. Supercell representing **1a** in simulations

References:

(1) I. D. Brown and D. Altermatt, *Acta Cryst. B*, 1985, **41**, 244-247.
(2) The density of pure liquid adsorbates and the vaporization heat of adsorbates were obtained from: *http://encyclopedia.airliquide.com/encyclopedia.asp*.
(3) Y. H. Hu and E. Ruckenstein, *Chem. Phys. Lett.*, 2006, **425**, 306-310.
(4) T. S. Jakubov and D. E. Mainwaring, *J. Colloid Interface Sci.*, 2002, **252**, 263-268.
(5) C. R. Reid and K.M. Thomas, *J. Phys. Chem. B*, 2001, **105**, 10619-10629.
(6) I. P. Okoye, M. Benham and K.M. Thomas, *Langmuir* 1997, **13**, 4054-4059.
(7) F.-X. Coudert, M. Jeffroy, A. H. Fuchs, A. Boutin, C. Mellot-Draznieks, *J. Am. Chem. Soc.* 2008, **130**, 14294-14302.
(8) C. Serre, S. Bourrelly, A. Vimont, N.A. Ramsahye, G. Maurin, P.L. Llewellyn, M. Daturi, Y. Filinchuk, O. Leynaud, P. Barnes and G. Férey, *Adv. Mater.*, 2007, **19**, 2246-2251.
(9) Z. Wang, and S.M. Cohen, *J. Am. Chem. Soc.*, 2009, **131**, 16675-16677.